Laser and Particle Beams (2007), *25*, 601–611. Printed in the USA.

DOI: 10.1017/S0263034607000717

Numerical simulations of the projectile ion charge difference in solid and gaseous stopping matter

S. EISENBARTH,[1] O.N. ROSMEJ,[1] V.P. SHEVELKO,[3] A. BLAZEVIC,[1] AND D.H.H. HOFFMANN[1,2]

[1]Gesellschaft für Schwerionenforschung mbH Darmstadt, Germany
[2]Institut für Kernphysik, Technische Universität Darmstadt, Darmstadt, Germany
[3]P.N. Lebedev Physical Institute, Moscow, Russia

(Received 18 June 2007; Accepted 22 August 2007)

Abstract

The dependence of calcium ion subshell populations on the target density during the ion stopping process was analyzed using a five charge-state collisional-radiative model. The model, which consists of the ground and three excited states for every ion charge, was successfully compared with the experiment. The gas-solid difference of calcium ion charge state distribution has been numerically demonstrated. For Ca projectiles with energies of 4–11 MeV/u, the increase of the mean ion charge in solid target is explained by the increase of the total ionization rate and by suppression of the bound electron capture process at high densities of the stopping medium.

Keywords: Collisional-radiative model; Gas-solid difference; Heavy ion stopping process; Ion charge state distribution; Ion subshells population kinetics; Projectile K-shell radiation

1. INTRODUCTION

The interaction of fast heavy ions with matter is a unique method to investigate processes in complex atomic systems, which play a very important role in modern atomic physics (Kawamura *et al.*, 2006; Nardi *et al.*, 2006). The current research in this field of science is motivated by the application of ion beams for well-tailored energy deposition in matter: inertial fusion, matter heating and tumor therapy (Labaune *et al.*, 2000; Hoffmann *et al.*, 2002, 2005; Deutsch & Popoff, 2006; Kraft, 2000).

The applications mentioned above require a detailed and precise knowledge of the energy deposition profiles as a function of projectile energy and the ion stopping range in the material. The target material can be either in solid, gas, liquid, or plasma state; also porous materials are a now days of considerable interest. It was demonstrated that the environment influences the energy deposition process (Nardi *et al.*, 2007; Barriga-Carrasco & Maynard, 2005; Hoffmann *et al.*, 1994). An enhanced energy loss and increased charge state of the projectiles was measured in experiments with plasma targets (Hoffmann *et al.*, 2000; Dietrich *et al.*, 1992).

Address correspondence and reprint requests to: Svitlana Eisenbarth, Gesellschaft für Schwerionenforschung mbH (GSI), Planckstrasse 1, D-64291 Darmstadt, Germany. E-mail: s.eisenbarth@gsi.de

Since the ion energy loss of heavy ions in matter is approximately proportional to the square of the ion mean charge, the knowledge about the dependency of the ion charge on the target material properties is of great importance. The first quantitative data about the difference in the charge state distribution of ions emerging from solid and gaseous targets were given by Lassen (1951*a*). His experimental work with uranium fission fragments clearly showed that the charge of projectiles emerging from thin carbon foils is higher than the charge of ions emerging from gases. He also found that the charge of ions emerging from gas increases with gas pressure increasing (Lassen, 1951*b*).

Bohr and Lindhard (1954) attempted to explain these experimental results (BL model). They related the observed gas-solid difference to the influence of the projectile excited states, which are highly populated if the projectile passes a solid target. Due to the difference in the binding energy of the ground and excited states, the effective ionization rates become higher, and thus lead to the increase of the ion charge state in dense stopping medium. At low target densities, collisional excitation of projectile electronic subshells will disappear due to spontaneous radiative transitions in the ion ground state before the next collision and ionization occur mostly from the ground state.

The BL model was verified experimentally for the high ion energy region. A detailed study was carried out at the

accelerator facility UNILAC/GSI (Darmstadt) using krypton, xenon, lead, and uranium projectiles in the energy range of 1–10 MeV/u (Geissel *et al.*, 1982). It was observed for the first time in experiments with 3.6–7.9 MeV/u uranium projectiles that the stopping power in gases is lower by up to about 20% than in solids.

The new experimental results on the increase of the effective ionization cross-section of 200 MeV/u nickel ions penetrating carbon foils were reported by Ogawa *et al.* (2007). The high energy was chosen in order to have simple systems, which are easier to treat theoretically. At this high energy only two nickel charge states with $Z = 28+$ and $27+$ survive at the level of some percent. The charge state distribution of nickel ions after interaction with a carbon foil and a nitrogen gaseous target was compared to each other. A 40% increase of the H-like fraction was detected and attributed to the increase of the total ionization rate in the solid material due to the high ionization cross section of the excited states.

In order to simplify the description of the ion electronic subshells in the stopping process, first theoretical works considered ions carrying only one or two bound electrons. Anholt formulated the four-state model of the population of bare and H-like ions via electron capture, ionization and excitation in collisions with target atoms (Anholt *et al.*, 1984; Anholt, 1985). A simpler three-state model containing *1s*, *2s*, and *2p* levels was solved by Anholt analytically. Calculations have shown that 19% of 400 MeV/u neon projectiles penetrating a Cu-target were excited to the *2s* and *2p* state. This has caused 30% of the gas-solid charge state difference. The influence of excited states of the projectile on the charge state of relativistic heavy ions was clearly demonstrated.

The strong influence of the projectile excited states on the ion charge state distribution in solid targets has been demonstrated by Rozet *et al.* (1996). The computer program ETACHE was developed to calculate the charge state distribution of ions with low Z, where electrons distributed over $n = 1$, 2, and 3 subshells, and for MeV/u projectile energies. The model predictions were in good agreement with experimental measurements for 13.6 MeV/u argon ions in carbon targets. Since the values of the radiative decay rates were introduced not directly but via fluorescence factors with insufficient accuracy, the model is restricted to solid density conditions and to projectiles with low atomic numbers, for which a de-excitation in solids occurs mostly nonradiatively.

The target density effect in collisions of fast ions with solid targets was analyzed in a series of papers by Shevelko *et al.* (2004, 2005). There, the target-density dependent formulas for electron capture and projectile ionization were obtained. It was shown that with the target density increasing electron capture cross-sections decrease and ionization cross-sections increase, resulting in a higher mean charge of exit ions after a solid target compared to a gas target. Using this treatment, a good agreement with experimental data on equilibrium charge-state fractions for projectile ions with atomic number $Z = 6$–26 passing through carbon foils was achieved in the MeV/u energy range.

In the present paper, we demonstrate the numerical calculations of the electronic subshell structure of calcium ions having been slowed down in SiO_2 media of different volume densities. These calculations were carried out in order to analyze experimental results for the dependence of the calcium projectiles K-shell radiation on the density of the stopping medium (Rosmej *et al.*, 2005*a*).

2. EXPERIMENT

2.1. Experimental Method

In order to analyze the projectile ion charge and velocity dynamics along the ion stopping path in the target, a novel diagnostic method, spatially resolved X-ray spectroscopy of the K-shell projectile radiation, has been applied (Rosmej *et al.*, 2002, 2003, 2005*b*). This method allows determining the projectile ion charge and velocity as a function of the ion penetration depth in the stopping medium. The high spectral ($\lambda/\Delta\lambda = 2000$–$5000$) and spatial (30–70 μm) resolutions were achieved using a spherically bend crystal spectrometer and Kodak X-ray films (Faenov *et al.*, 1994; Rosmej *et al.*, 2002).

The spectroscopic method is based on measurements of the characteristic K-shell emission of projectile ions excited in close collisions with target atoms (Kauffman *et al.*, 1976). At close-to-zero impact parameters, the probability of the K-shell electron ionization and production of the projectile K-shell vacancy is rather high and depends only slightly on the ion charge state (Rosmej *et al.*, 2005*a*). The resulting autoionizing states are very unstable and can decay via two noncollisional processes—Auger ionization or resonant radiative decay of one of the bound electrons into the K-shell vacancy. In the case of middle Z elements, the time scale of both processes is some tens of femtoseconds (Safronova & Lisina, 1979), therefore, de-excitation occurs after the projectile has passed about 500 nm of the stopping medium. Since this is beyond the spatial resolution provided in the experiments, one can suggest that processes of the ion excitation (ionization) in collisions with target atoms and K_α-radiation occur from the same part of interaction region.

The energy of the K-shell radiative transitions in ions with different charges does not vary significantly due to shielding effects produced by projectile bound electrons at higher subshells. For example, the wavelength of the K_α-transition in an H-like calcium ion (*1s-2p*) is 0.301 nm, in a Li-like Ca ($1s^2 2s$-$1s2s2p$) is 0.318 nm, and in an F-like ($1s^2 2s^2 2p^3$-$1s2s^2 2p^4$) is 0.336 nm. This feature allows us, from one side, to register the K-shell radiation of all projectile charge states by the same X-ray spectrometer, and from the other side, to demand spectral resolution of the detector higher then $\lambda/\delta\lambda = 1000$. The line intensity distribution of the K-shell transitions arising from ions with different ion

https://doi.org/10.1017/S0263034607000717 Published online by Cambridge University Press

charges represents the charge state distribution. The redistribution of the intensities of the K-shell satellites, arising from different ion charge states with the penetration depth in the target, demonstrates the ion charge state evolution along the ion beam stopping path.

The spectroscopic method discussed above was used in experiments on the penetration of a $^{48}Ca^{10+}$ ion beam with initial energies of 5.9 MeV/u and 11.4 MeV/u into solid, foam, and gaseous targets. Experiments on the interaction of heavy ion beams with different types of targets were carried out at the Universal Linear Accelerator (UNILAC) of the Gesellschaft für Schwerionenforschung (GSI, Darmstadt). The detailed experimental setup is described by Rosmej *et al.* (2002, 2003, 2005*a*).

2.2. K-shell Spectra of Calcium Ions Penetrating SiO_2 Low-Density Aerogel

In experiments mentioned above, the dependence of the projectile ion K-shell spectra on the penetration depth in the stopping material was measured. Figure 1 show a typical experimental spectrum of Ca projectiles, which have been slowed down in a porous SiO_2 target of 0.023 g/cm^3 mean density.

The use of porous stopping media with a volume density up to 100 times lower than of amorphous quartz ($\rho =$ 2.3 g/cm^3) allowed stretching the ion stopping path and resolving the evolution of the K-shell projectile ion and target radiation along the ion trajectory (Rosmej *et al.*, 2002, 2003, 2005*a*).

If the high energy monocharged ion beam passes through a solid target, it is ionized in collisions with target atoms. The charge state distribution corresponding to the current projectile velocity will be established at the first hundreds of nanometers in the target. In the spectrum, one can observe intensive K-shell radiation of highly charged H- *(1s-2p)* and He-like *($1s^2$-1s2p)* calcium ions at the beginning of the ion stopping path (Fig. 1a). Penetrating into the target and loosing the energy ions start to capture bound target electrons. The spectrum at the end of the observed ion stopping path displays the K-shell transitions toward lower charged ions such as Li-*($1s^2$2l-1s2l2l)* and Be-like *($1s^2$2l2l-1s2l2l2l)* (Fig. 1b). Therefore, K-shell spectra spatially resolved along the ion path in the target "visualize" the evolution of the ion charge state during the ion stopping process.

Another interesting feature of the spatially resolved projectile spectra is a tilted form of the spectra lines. Radiation of ions moving with 1/10 of the speed of light exhibits a relativistic Doppler shift. The value of the shifted wavelength is proportional to the ion velocity. During the penetration in a stopping medium, the ion velocity and therefore the Doppler shift are decreasing continuously imaging the deceleration process. A high spectral resolution ($\lambda/d\lambda =$ 3000) of the spherically bend mica spectrometer (Faenov *et al.*, 1994) allows obtaining the ion velocity dependence with the penetration depth using the Doppler line shift with

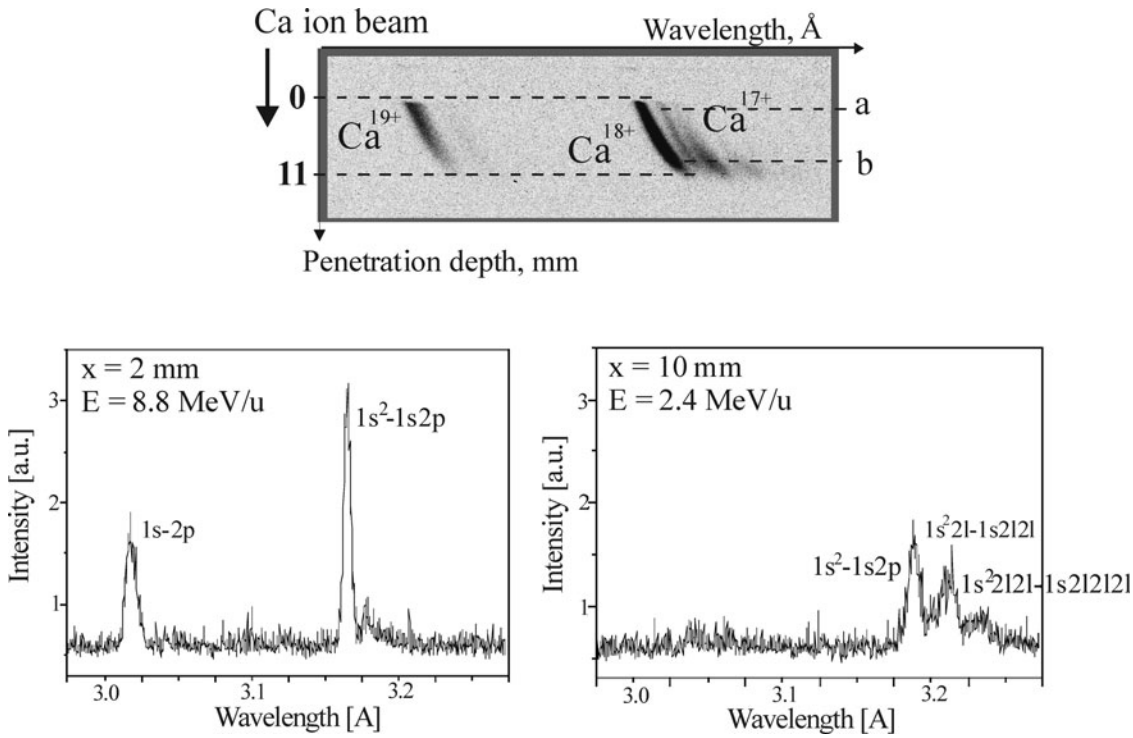

Fig. 1. K-shell spectrum of Ca ions with an initial energy of 10.7 MeV/u slowed down in 0.023 g/cm^3 SiO_2 aerogel. Densitograms demonstrate the evolution of the K_α-satellite spectra with a penetration depth. The ion energy corresponding to the penetration depth is defined from the Doppler line shift.

https://doi.org/10.1017/S0263034607000717 Published online by Cambridge University Press

accuracy of 7%. The method was proved using time-of-flight measurements (Rosmej *et al.*, 2005*a*).

In order to prove the validity of the applied spectroscopic method for the investigation of the ion charge state evolution, the measurements were complemented by the analysis of the charge state distribution of Ca ions emerging from the target. Figure 2a depicts the charge state distribution of Ca ions with a final energy of 6.5 MeV/u after emerging from 8.39 mm thick piece of 0.023 g/cm^3 SiO_2 aerogel target. The results are obtained using a 1.63T magnet spectrometer. The ion beam energy behind the target measured by means of the time-of-flight method was of 6.5 MeV/u (Rosmej *et al.*, 2005*a*; Fertman *et al.*, 2006).

Simultaneously, the spatially resolved K-shell spectra were registered. The radiation was observed at 90 degrees with respect to the ion beam axis. Figure 2b shows the characteristic lines occurring due to radiative transitions from one and double excited states *2p, 1s2p*, *1s2p2p* in Ca^{19+}–Ca^{17+} ions before the projectiles left the target.

The results of these two methods cannot be compared directly since the method of X-ray spectroscopy provides the measurement of the population only of excited ion states with a K-shell vacancy inside the stopping medium. A magnet spectrometer however measures the distribution of the ions over the ground states outside the interaction region.

Numerical simulations have been performed in order to conclude about the charge state distribution of ions inside the target material using the experimental results of the K-shell spectroscopy.

3. POPULATION KINETICS OF THE PROJECTILE GROUND AND EXCITED STATES

A quantitative analysis of the projectile ion population kinetics governed by ion–target atom collisions and noncollisional processes has been performed in order to predict the charge state distributions of fast heavy ions inside stopping matter.

The fraction of projectiles having the charge Z is defined as a sum over the population density of the ion ground and excited states. With growing target density, the population of excited ions starts to be comparable with those in the ground state. The last one influences the total ionization and electron capture cross-sections and leads to the observed dependence of the projectile ion charge state distribution on the target density.

Line intensities of the characteristic projectile spectra measured in the experiments are directly proportional to the populations of excited states with K-shell vacancies giving rise to the corresponding radiative transitions. Therefore, the population of the ion excited states can be measured directly.

The intensity of a spectral line corresponding to the transition from the upper energy level k to the lower i of an atom is given by (Sobelman & Vainshtein, 2006):

$$I_{ki} = \hbar\,\omega_{ki} A_{ki} P(k) \quad \lfloor eVs^{-1}cm^{-3} \rfloor, \tag{1}$$

where A_{ki} is the radiative probability for the transition $k \rightarrow i$, $P(k)$ is the population density of ions excited to the level k, ω_{ki} is the frequency of the transition, and $\hbar$ is Planck's constant divided by 2π. The population of the ion ground states cannot be directly measured inside the stopping medium using projectile self radiation. Hence, it will be then predicted by means of the numerical procedure taking into account all elementary collisional and noncollisional processes connecting the ground and excited states and their dependence on the ion energy, ion charge and density of the stopping matter.

3.1. Collisional and Noncollisional Processes In Projectile Ion–Target Atom Interactions

In order to estimate the distribution of ions over their energy levels due to collisions with target atoms, the following elementary atomic processes have to be taken into account: electron capture and loss (charge exchange), collisional excitation and de-excitation as well as radiative, and Auger decays.

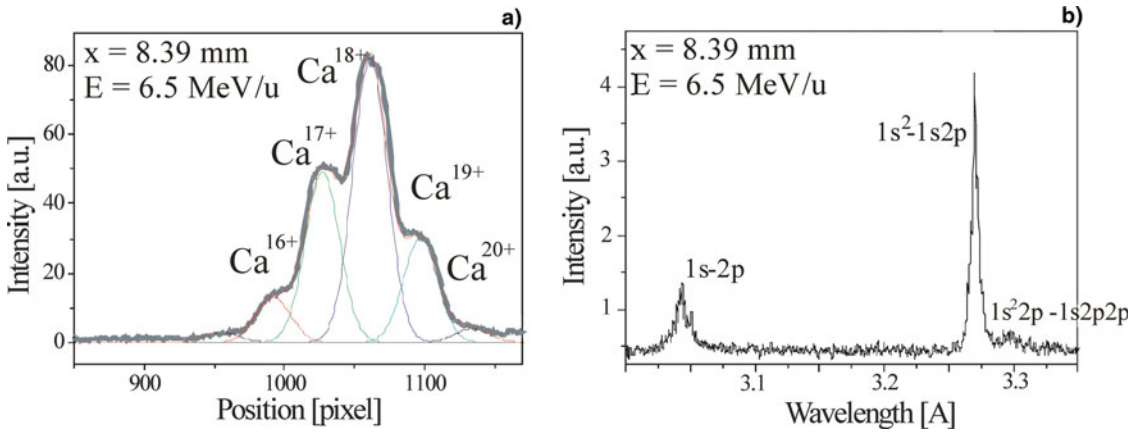

Fig. 2. (Color online) Experiments on the interaction of 11.4 MeV/u Ca ions with a 8.39 mm thick piece of 0.023 g/cm^3 SiO_2 aerogel. (**a**) The charge state distribution of Ca ions measured after the target by means of a magnetic spectrometer. (**b**) Ca-K_α-radiation observed inside the stopping medium using the X-ray spectroscopy.

https://doi.org/10.1017/S0263034607000717 Published online by Cambridge University Press

Bound electron capture cross-sections were calculated using the CAPTURE code described in the papers by Shevelko *et al.* (2001) and Shevelko *et al.* (2004). In this code cross-sections of one-electron charge exchange are calculated using the method of multichannel normalization of the capture probabilities in the impact parameter representation. This method employs the relationship between the quasi-classical and the quantum-mechanical charge exchange amplitudes (Shevelko, 1980). Results of these calculations are presented in Figure 3.

The LOSS code (Shevelko *et al.*, 2001) was used to calculate one-electron ionization cross-sections of fast ions colliding with neutral atoms in the momentum transfer representation in the first Born approximation with account of the atomic structure of the target. Calculated by the LOSS code K-shell ionization cross-sections of Ca^{Z+} ions colliding with SiO_2 molecules are presented in Figure 4. The computer code also allows estimating the excitation cross-sections of projectiles by the target atoms and molecules. Cross-sections of the de-excitation process were calculated using the principle of detailed balance (the Klein-Rosseland relation) (Klein & Rosseland, 1921). In calculations of the charge-changing cross-sections for projectiles colliding with molecule targets, the Bragg's additivity rule was used.

The radiative transition probabilities were calculated using the classical approximation (Lebedev & Beigman, 1998)

$$A(n_1 - n_0) \approx 1.61 \times 10^{10} \frac{(Z+1)^4}{n_1^3 n_0} \frac{1}{\Delta n (n_1 + n_0)} \left(1 - \frac{0.236}{\Delta n}\right),$$
$$n_{0,1} = \left(\sqrt{E_{0,1}/(Z+1)^2\, Ry}\right)^{-1}, \Delta n = n_1 - n_0, \quad (2)$$

where $E_{0,1}$ is the ion energy levels counted from the ionization limit, Z is the ion charge, n_1 and n_0 are the principle quantum numbers of the upper 1 and lower 0 levels, respectively.

3.2. Five State-Collisional-Radiative Model

Numerical calculations of population density of Ca ions colliding with SiO_2 target atoms have been performed using the energy level system presented in Figure 5. The chosen model was limited to Ca^{20+}–Ca^{15+} ions since the observed K-shell spectra in the experiments correspond to the ion charges of $Z = 16–19$. For every ion charge state, the ground and three excited states without spin-orbital splitting were considered. Autoionizing (double excited) states were neglected in the considered energy level system, since at high projectile velocities they are weekly populated and made no influence on the ion charge fraction in comparison to the ground and nearby states.

We assume that the distribution inside the same principal quantum number n follows the statistical law that is the case at high densities of the stopping material. The distribution of the population fractions over the ion energy levels is described by a system of the rate equations of the multilevel kinetics. The differential equation for the fraction P of the energy level k of the ion Z can be written as

$$\frac{dP_Z(k)}{dt} = \sum_{Z'} \sum_i B_{ik} P_{Z'}(i) - B_{kk} P_Z(k), \quad (3)$$

where $P_{Z'}(i)$ is the population fraction of the level i of the ion charge Z'; B_{ik} are rate coefficients of the atomic

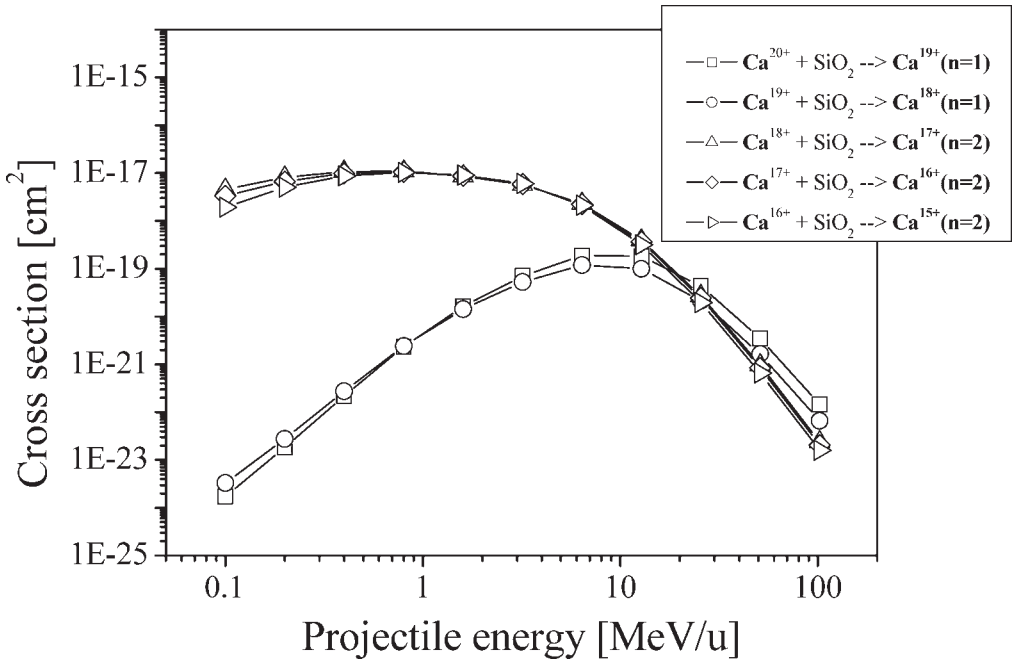

Fig. 3. Dependence of the bound electron captures cross sections for Ca^{Z+} ion ground state in collisions with SiO_2 molecules on the ion energy. The calculations were performed using the CAPTURE code.

https://doi.org/10.1017/S0263034607000717 Published online by Cambridge University Press

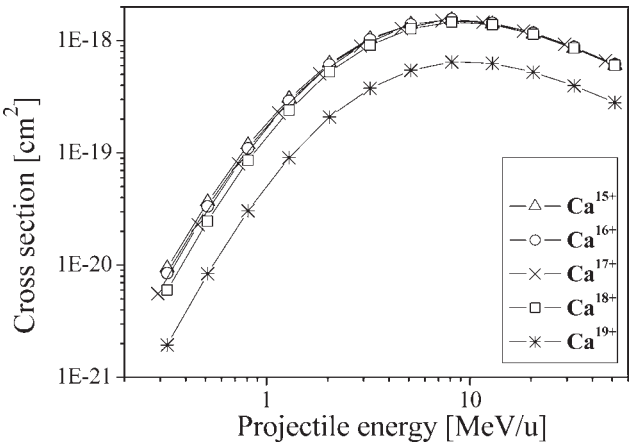

Fig. 4. *K*-shell ionization cross sections of Ca^{Z+} ions colliding with SiO_2 molecules as a function of the projectile energy calculated using the LOSS code.

processes occurring between the level k of the ion Z and the level i of the ion Z'; B_{kk} denotes the sum of the atomic processes, which depopulate the energy level k of the ion Z. The time is coupled to the coordinates by the projectile velocity.

In atomic physics, the rate of collisional process is given as

$$R_{coll} = N_T \upsilon \sigma_{coll}, \tag{4}$$

where N_T is the target density in at/cm^3, υ is the projectile velocity, and σ_{coll} is the cross-section of the collisional process in cm^2. The quantity R_{coll} characterizes the number of interactions per time unit and has the dimension of s^{-1}. The rate coefficient of the noncollisional processes is introduced by the radiative decay rate A in s^{-1}.

Since the rates of collisional processes are directly proportional to the target density, and radiative decay rates are characterized only by the ion energy level structure, the dependence of the ion population over excited states on the target density takes place.

The population fraction $P_Z(k)$ is defined from equilibrium state $dP_Z(k)/dt = 0$:

$$P_Z(k) = \frac{\sum_{Z'} \sum_{i} B_{ik} P_{Z'}(i)}{B_{kk} P_Z(k)}, \tag{5}$$

The system of 21 linear equations in regard to $P_Z(k)$ has been solved. The set of differential equations was considered in the form of a matrix equation $BP = a$. B is the matrix of collisional and noncollisional rate coefficients, which connects the ground and excited states of ions and is written by

$$B = \begin{pmatrix} -b_{11} & b_{12} & \cdots & b_{1m} \\ b_{21} & -b_{22} & \cdots & b_{2m} \\ \cdots & \cdots & \cdots & \cdots \\ b_{m1} & b_{m2} & \cdots & -b_{mm} \end{pmatrix}. \tag{6}$$

The column vector P denotes populations of the energy states:

$$P = \begin{pmatrix} P(1) \\ P(2) \\ \cdots \\ P(m) \end{pmatrix}. \tag{7}$$

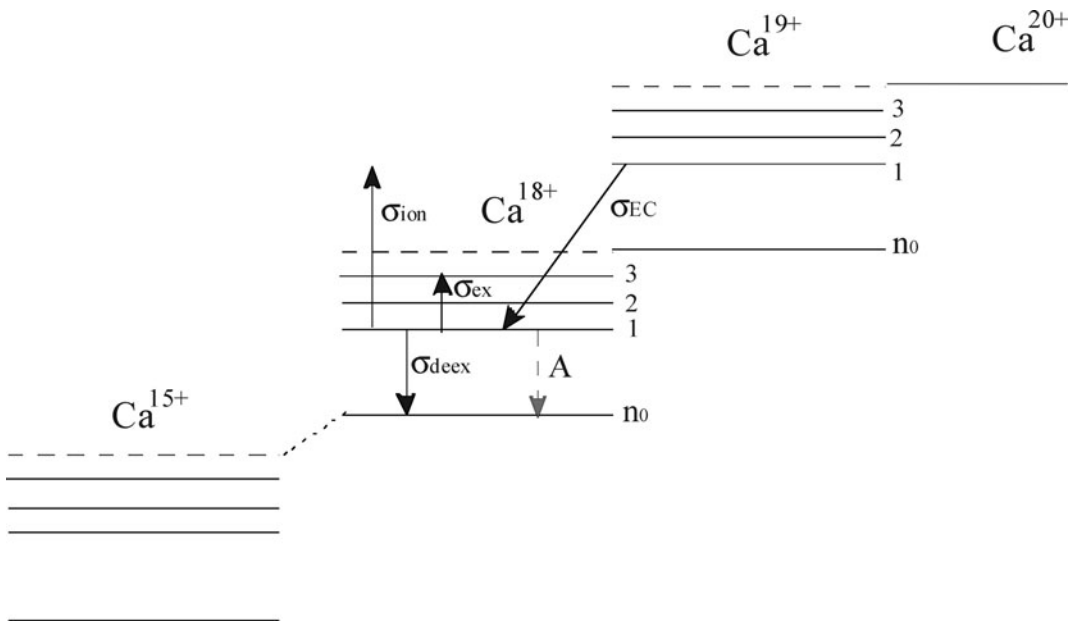

Fig. 5. Schematic drawing of the atomic population kinetics model.

https://doi.org/10.1017/S0263034607000717 Published online by Cambridge University Press

Since $dP_Z(k)/dt = 0$, the vector is equal 0. At $-B_{kk} = \sum_{i \neq k} B_{ik}$ the matrix system is singular. Therefore, one of the equations was replaced by the conservation law of the number of particles, $\sum_{Z,k} P_Z(k) = 1$. The system of linear equations

$$\begin{pmatrix} -b_{11} & b_{12} & \cdots & b_{1m} \\ b_{21} & -b_{22} & \cdots & b_{2m} \\ \cdots & \cdots & \cdots & \cdots \\ 1 & 1 & \cdots & 1 \end{pmatrix} \begin{pmatrix} P(1) \\ P(2) \\ \cdots \\ P(m) \end{pmatrix} = \begin{pmatrix} a_1 \\ a_2 \\ \cdots \\ 1 \end{pmatrix} \tag{8}$$

was solved with respect to *P(m)* using the Gaussian elimination method.

3.3. Comparison with experiments

The validity of the numerical calculations of the population kinetics has been compared with measurements. The charge state distribution of Ca ions after emerging from 8.39 mm thick peace of 0.023 g/cm^3 silica aerogel performed by means of a magnetic spectrometer was compared with calculations at the same ion energy of 6.5 MeV/u. The results are shown in Figure 6. In order to notice the difference between measurements and calculations, the numbers are presented in Table 1. The fraction of projectile ions with a charge Z was defined as the sum over the population density of the ion ground and excited states.

Measurements of the ion charge states after the stopping medium were accomplished by a spatially resolved spectroscopic analysis of the projectile radiation (Fig. 2b). The calculated relative intensities of Ly_α (Ca^{19+}) and He_α (Ca^{18+}) characteristic lines at the ion energy of 6.5 MeV/u before the ion beam left the target coincide very well with experimental ratio (Table 2).

In conclusion, we would like to note that the numerical calculations are in close agreement with experimental measurements of the charge state distribution of calcium ions inside and behind a stopping medium. The described collisional-radiative model is capable to predict the ion charge evolution during the energy loss process under different stopping conditions. Using the measured dependence of the projectile velocity on the ion penetration depth for the calculation of rate coefficients of collisional processes it is now possible to analyze the behavior of the projectile K-shell radiation along the ion stopping path in the target material.

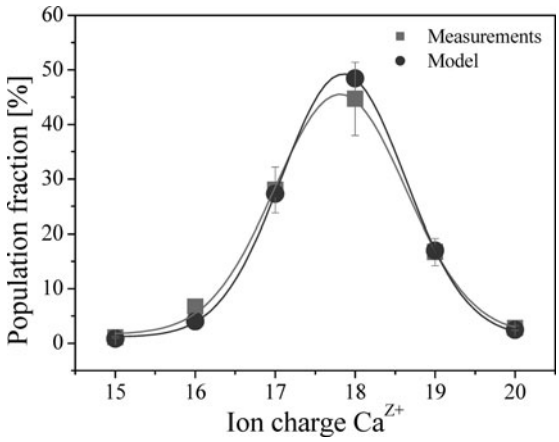

Fig. 6. Calcium ion charge state distribution measured by a magnetic spectrometer after the aerogel target and calculated using the collisional-radiative model at the projectile energy of 6.5 MeV/u.

Table 1. *The population fractions of calcium ions obtained by the magnet measurements and numerical calculations*

Ion charge	Population (fractions, %)	
	Magnet measurements	Calculations
Ca^{20+}	2.8	2.71
Ca^{19+}	16.7	17.8
Ca^{18+}	44.7	48.2
Ca^{17+}	28.0	26.6
Ca^{16+}	6.7	3.86
Ca^{15+}	1.1	0.74

3.4. Dependence of the Calcium Ion Subshell Structure on the Target Density. Results and Discussion

The influence of the target density on the population of the projectile ion subshells is governed by the competition between collisional and noncollisional processes responsible for the depopulation of excited bound electrons. For a better understanding of this problem, let us introduce the quenching factor $\beta(n)$, which is defined as the ratio of the collisional and radiative rates for the depopulation of the ion excited state with a principal quantum number n:

$$\beta(n) = \frac{R_{coll}(n)}{A(n)} = \frac{\upsilon \sigma_{coll}(n) N_T}{A(n)}, \tag{9}$$

where υ is the ion velocity, σ_{coll} is the collisional depopulation cross section, N_T is the target density, and A is the radiative decay rate. Collisional depopulation can occur via de-excitation to lower energy levels and due to further excitation or ionization into continuum. Let us consider the dependence of the quenching factor on the most important projectile ion and target parameters.

Table 2. *Measured and calculated data of relative line intensities for the experiment on the interaction of Ca ions with a 8.39 mm thick piece of 0.023 g/cm^3 SiO_2 aerogel (Fig. 2b)*

$I(Ly_\alpha)/I(He_\alpha)$	Measurements	Calculations
6.5 MeV/u	0.32	0.37

https://doi.org/10.1017/S0263034607000717 Published online by Cambridge University Press

The corresponding ionization and radiative rate coefficients can be scaled as

$$R_{coll}(n) \propto \frac{N_T n^2}{Z^2 v}, \tag{10}$$

$$A(n) \propto \frac{(Z+1)^4}{n^5}, \tag{11}$$

where Z is the ion charge and n is the principal quantum number of the ion excited state.

Therefore, for the quenching factor one obtains the following dependence:

$$\beta(n) \propto \frac{N_T n^7}{Z^6 v}. \tag{12}$$

As follows from Eq. 12, the factor $\beta(n)$ grows strongly with the increase of the principal quantum number n of the excited bound electron and with the target density, and decreases with the projectile velocity and the ion charge.

In Figure 7 we have plotted quenching factors for H-like 6 MeV/u Ca ions colliding with SiO_2 of different target densities. In the calculations, collisional and radiative processes were taken into account, which depopulate Ca^{19+} excited energy levels with principal quantum numbers $n = 1, 2, 3$.

The quenching factor $\beta = 1$ means that 50% of the excited bound electrons decay radiatively to the ground state and 50% are ionized or excited to the higher ion levels.

Figure 7 demonstrates that practically all excited electrons populating $n = 1, 2, 3$ levels in H-like Ca^{19+} ions undergo the radiative relaxation to the ground state *1s* at the target density of 10^{19} at/cm^3.

At higher target densities, when the quenching factor is larger then 1, the depopulation of the excited states is governed mostly by collisional processes. This leads to the increased population of excited states with respect to the ion ground state as one can see in Figure 8.

With growing target densities, the population of the excited ions becomes comparable to the ground one since the time between collisions is short to allow the radiative relaxation to the ground state. Successive collisions of excited ions with target atoms lead to additional and very effective channels of ionization and result in the increase of the total ionization rate:

$$\sigma_{ion}^{total} = P_{n0}\sigma_{ion}(n_0) + P_n^*\sigma_{ion}(n) + P_{n+1}^*\sigma_{ion}(n+1) + \ldots, \tag{13}$$

where P_{n0} and P_n* are the population densities of the ground and excited states, respectively; σ_{ion} *(n)* is the ionization cross-section from the level with the principal quantum number n. Due to low binding energies of the excited energy levels, the ionization cross-sections $\sigma_{ion}(n)$ can be much higher than those for the ion ground state $\sigma_{ion}(n_0)$. At low target densities, P_n^* is negligible compared to the ground state (Fig. 6), and the ionization is defined by the first term $P_{n0}\sigma_{ion}(n_0)$ in Eq. (13). With growing target density, the total ionization cross-section exceeds the total cross section calculated for the low density case by a factor of ten and more (Fig. 9).

Collisions influence not only the effective ionization cross-sections, but lead as well to the suppression of the bound electron capture to the projectile excited states. At low ion energies, target electrons can be captured with a high probability to the projectile excited state having quenching factors bigger than 1. High rates of collisional depopulation prevent the stabilization of the capture process via relaxation to the ground state: captured target electrons will be immediately ionized (Shevelko *et al.*, 2005).

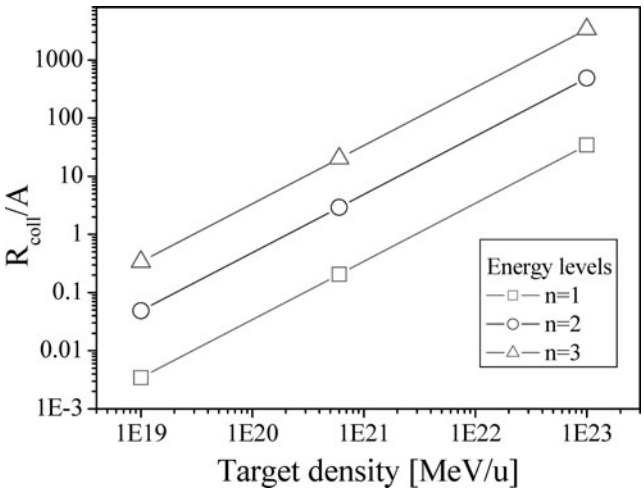

Fig. 7. Quenching factors $\beta(n)$ calculated for three excited states ($n = 1, 2, 3$) of 6 MeV/u Ca^{19+} ions as a function of SiO_2 target density.

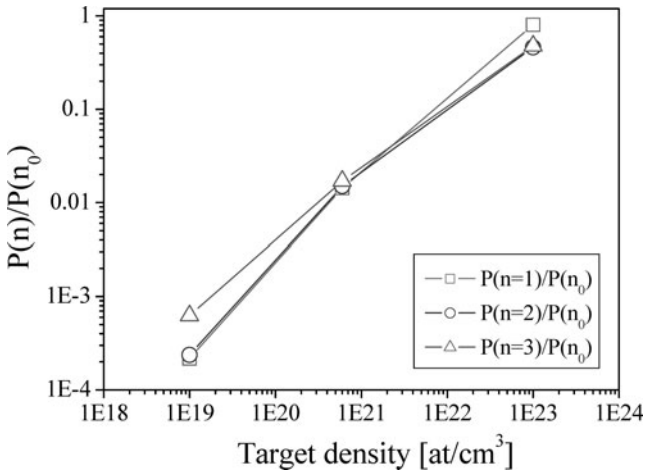

Fig. 8. Population density $P(n)$ of 6 MeV/u Ca^{19+} ions calculated for three excited ($n = 1, 2, 3$) states and normalized with respect to the population of the ground state $P(n_0)$.

https://doi.org/10.1017/S0263034607000717 Published online by Cambridge University Press

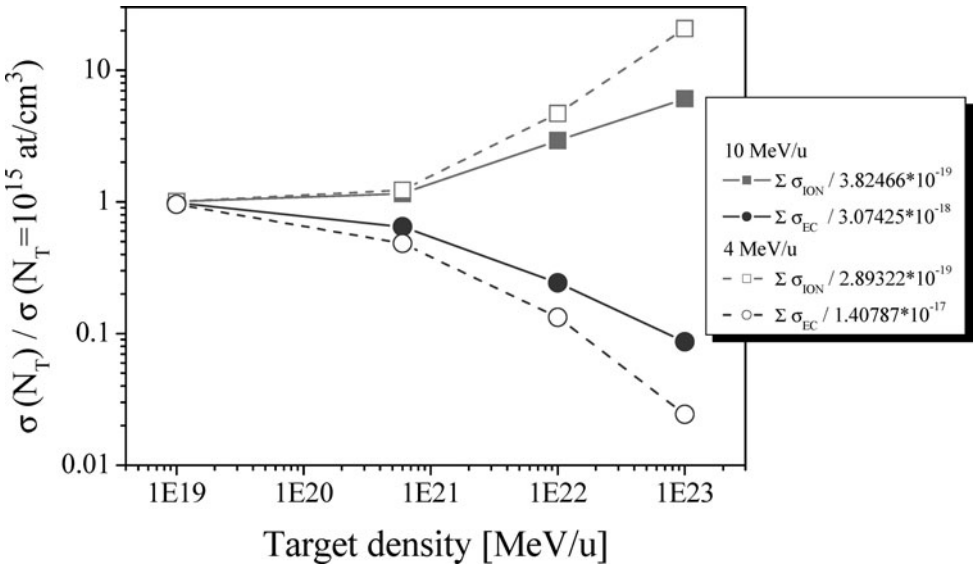

Fig. 9. Calculated total ionization and bound electron capture cross sections of Ca^{19+} ions interacting with SiO_2 atoms as a function of the target density. They are normalized to the cross sections at very low target density 10^{15} at/cm^3, at which the depopulation of the excited levels is governed by radiative processes.

Calculations of the total ionization and recombination cross-sections for H-like Ca ions interacting with SiO_2 medium of different densities are presented in Figure 9.

Total ionization cross-sections were calculated according to Eq. (13), while the total captures cross-sections according the following equation:

$$\sigma_{EC}^{total} = \sum_n \sigma_{EC}(n)/(1+\beta(n)), \tag{14}$$

where $\sigma_{EC}(n)$ is the cross-section of the bound electron capture to the ion level with a principal quantum number n, $\beta(n)$ is the quenching factor for this level. The populations of the ion ground and excited states as well as quenching factors were calculated using the described collisional–radiative model. From Eq. (14) one can see that only capture to the ion excited levels with low damping factors contributes to the charge change process.

The influence of collisional processes on the total bound electron capture cross-sections is more effective at lower projectile energies since the target electron will be captured to the higher excited level n with a quenching factor growing as n^7. From Figure 9 one can see that at 4 MeV/u ion energy and solid target density, the capture process is 50 times less effective than at the density corresponding to 1 bar gas pressure. For Ca^{19+} ions of 10 MeV/u it is only a factor of 10.

The increase of the total ionization rates and the suppression of the capture processes at high target densities lead to an increase of the ion charge state inside the stopping medium. Equilibrium charge state distributions of 6 MeV/u Ca ions in a solid quartz of 10^{23} at/cm^3 density and a gaseous target of 10^{19} at/cm^3 density have been calculated by means of the described collisional-radiative model. The results are presented in Figure 10. The Ca ion mean charge in solid matter is of $\langle Z\rangle = 19.1$, while in gaseous one is of $\langle Z\rangle = 17.34$.

The calculated equilibrium mean charge in solid SiO_2 is in good agreement with measurements of Shima (Shima *et al.*, 1982) giving $\langle Z\rangle = 18.57$ for 6 MeV/u Ca ions penetrating a carbon foil. The difference can be explained by the dependence of collisional cross sections on the target atomic number.

4. CONCLUSION

A quantitative analysis of the ion subshells population kinetics in the projectile–target interaction process has been

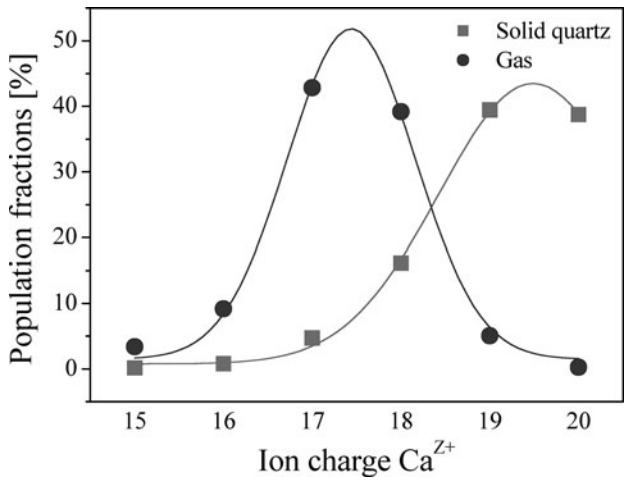

Fig. 10. Equilibrium charge state distributions of 6 MeV/u Ca ions in solid quartz (10^{23} at/cm^3) and gaseous medium (10^{19} at/cm^3) calculated using the five-state model.

https://doi.org/10.1017/S0263034607000717 Published online by Cambridge University Press

performed. A five charge-state collisional-radiative model has been created, which considers the ground and three excited states for each ion charge. Numerical calculations account for collisional and noncollisional processes of the ion population kinetics for 21 ground and excited states, and allowed the prediction of the projectile charge state distribution inside stopping medium.

The model was satisfied compared with the ion charge state distribution measured after the SiO_2 foam target by means of a magnet spectrometer. The calculations have shown a good agreement with the measured projectile K-shell spectra.

The gas-solid difference of the ion charge state distribution has been numerically demonstrated. The calculations have shown that the increase of the ion charge in a solid target can be explained by the increase of the total ionization rate, and the suppression of the bound electron capture process. The suppression of the bound electron capture starts to be dominant at the ion velocity providing the capture to the ion excited states with large damping factors β.

Summarizing we would like to stress out, that the selection of proper experimental conditions for a demonstration of the gas-solid effect requires a detailed knowledge of the rates of elementary processes governing the population of ion electronic subshells.

ACKNOWLEDGMENT

This work has been supported by the project BMBF 06 DA 116.

REFERENCES

Anholt, R., Meyerhof, W.E., Stoller, C., Morenzoni, E., Andriamonje, S.A., Molitoris, J.D., Baker, O.K., Hoffmann, D.H.H., Bowman, H., Xu, J.S., Xu, Z.Z., Frankel, K., Murphy, D., Crowe, K. & Rasmussen, J.O. (1984). Atomic collisions with relativistic heavy ions: Target inner-shell ionization. *Phys. Rev. A* **30**, 2234–2244.

Anholt, R. (1985). Atomic collisions with relativistic heavy ions. II. Light-ion charge states. *Phys. Rev. A* **31**, 3579–3592.

Barriga-Carrasco, M.D. & Maynard, G. (2005). A 3D trajectory numerical simulation of the transport of energetic light ion beams in plasma targets. *Laser Part. Beams* **23**, 211–217.

Bohr, N. & Lindhard, J. (1954). Electron capture and loss by heavy ions penetrating through matter. *Dan. Mat. Fys. Medd.* **28**, 1–31.

Deutsch, C. & Popoff, R. (2006). Low velocity ion stopping of relevance to the US beam-target program. *Laser Part. Beams* **24**, 421–425.

Dietrich, K.G., Hoffmann, D.H.H., Boggasch, E., Jacoby, J., Wahl, H., Elfers, M., Haas, C.R., Dubenkov, V.P. & Golubev, A.A. (1992). Charge state of fast heavy ions in a hydrogen plasma. *Phys. Rev. Lett.* **69**, 3623–3626.

Faenov, A.Ya., Pikuz, S.A., Erko, A.I., Bryunetkin, B.A., Dyakin, V.M., Ivanenkov, G.V., Mingaleev, A.R., Pikuz, T.A., Romanova, V.M. & Shelkovenko, T.A. (1994). High-performance X-ray spectroscopic devices for plasma microsources investigations. *Phys. Scrip.* **50**, 333–338.

Fertman, A., Mutin, T.Yu., Turtikov, V.I., Blazevic, A., Efremov, V.P., Golubev, A.A., Hoffmann, D.H.H., Korostiy, S., Pikuz jr., S.A., Rosmej, O.N. & Sharkov, B.Yu. (2006). Stopping of calcium ions in low density SiO_2 aerogels. *33rd EPS Conf. on Plasma Phys. Rome* (30I), 2.001.

Geissel, H., Laichter, Y.Schneider, W.F.W. & Armbruster, P. (1982). Energy loss and energy loss straggling of fast heavy ions in matter. *Nucl. Instr. Meth.* **194**, 21–29.

Hoffmann, D.H.H., Jacoby, J., Laux, W., Demagistris, M., Boggasch, E., Spiller, P., Stockl, C., Tauschwitz, A., Weyrich, K., Chabot, M. & Gardes, D. (1994). Energy loss of fast heavy ions in plasmas. *Nucl. Instr. Meth. Phys. Res. B* **90**, 1–9.

Hoffmann, D.H.H., Bock, R., Faenov, A.Ya., Funk, U., Geissel, M., Neuner, U., Pikuz, T.A., Rosmej, F., Roth, M., Süß, W., Tahir, N. & Tauschwitz, A. (2000). Plasma physics with intense laser and ion beams. *Nucl. Instr. Meth. Phys. Res. B* **161**, 9–18.

Hoffmann, D.H.H., Fortov, V.E., Lomonosov, I.V., Mintsev, V., Tahir, N.A., Varentsov, D. & Wieser, J. (2002). Unique capabilities of an intense heavy ion beam as a tool for equation-of-state studies. *Phys. Plasmas* **9**, 3651–3654.

Hoffmann, D.H.H., Blazevic, A., Ni, P., Rosmej, O., Roth, M., Tahir, N.A., Tauschwitz, A., Udrea, S., Varentsov, D., Weyrich, K. & Maron, Y. (2005). Present and future perspectives for high energy density physics with intense heavy ion and laser beams. *Laser Part. Beams* **23**, 47–53.

Kauffman, R.L., Jamison, K.A., Gray, T.J. & Richard, P. (1976). Heavy-ion-produced high–resolution Si-*K*-X-ray spectra from a gas and solid. *Phys. Rev. Lett.* **36**, 1074–1077.

Kawamura, T., Horioka, K. & Koike, F. (2006). Potential of K_α radiation by energetic ionic particles for high energy density plasma diagnostics. *Laser Part. Beams* **24**, 261–267.

Klein, O. & Rosseland, S. (1921). Über Zusammenstöße zwischen Atomen and freien Elektronen. *Z. Phys. A* **4**, 46–51.

Kraft, G. (2000). Tumor therapy with heavy charged particles. *Prog. Part. Nucl. Phys.* **45**, 473–544.

Labaune, C., Hogan, W.J. & Tanaka, K.A. (2000). *Proceeding of "First International Conference on Inertial Fusion Science and Application"* Paris: Elsevier.

Lassen, N.O. (1951*a*). The total charges of fission fragments in gaseous and solid stopping media. *Dan. Mat. Fys. Medd.* **26**, 1–28.

Lassen, N.O. (1951*b*). Total charges of fission fragments as functions of the pressure of the stopping gas. *Dan. Mat. Fys. Medd.* **26**, 1–19.

Lebedev, V.S. & Beigman, I.L. (1998). *Physics of Highly Excited Atoms.* Berlin: Springer.

Nardi, E., Fisher, D.V., Roth, M., Blazevic, A. & Hoffmann, D.H.H. (2006). Charge state of Zn projectile ions in partially ionized plasma: Simulations. *Laser Part. Beams* **24**, 131–141.

Nardi, E., Maron, Y. & Hoffmann, D.H.H. (2007). Plasma diagnostics by means of scattering of electron and proton beams. *Laser Part. Beams* **25**, xxx–xxx.

Ogawa, H., Geissel, H., Fettouhi, A., Fritzsche, S., Pottillo, M., Scheidenberger, C., Shevelko, V.P., Surzhykov, A., Weick, H., Becker, F., Boutin, D., Kindler, B., Knöbel, R.K., Kurcewicz, W., Litvinov, Yu.A., Lommel, B., Münzenberg, G., Plaß, W.R., Sakamoto, N., Stadlmann, J., Tsuchida, H.,

Winkler, M. & Yao, N. (2007). Gas-solid difference in charge-changing cross sections for bare and H-like nickel ions at 200 MeV/u. *Phys. Rev. A* **75**, 020703.

Rosmej, O.N., Wieser, J., Geissel, M., Rosmej, F., Blazevic, A., Jacoby, J., Dewald, E., Roth, M., Brambrink, E., Weyrich, K., Hoffmann, D.H.H., Pikuz, T.A., Faenov, A.Ya., Magunov, A.I., Skobelev, I.Y., Borisenko, N.G., Shevelko, V.P., Golubev, A.A., Fertman, A., Turtikov, V. & Sharkov, B.Y. (2002). X-ray spectromicroscopy of fast heavy ions and target radiation. *Nucl. Instr. Meth. Phys. Res. A* **495**, 29–39.

Rosmej, O.N., Pikuz jr., S.A., Wieser, J., Blazevic, A., Brambrink, E., Roth, M., Efremov, V.P., Faenov, A.Ya., Pikuz, T.A., Skobelev, I.Yu. & Hoffmann, D.H.H. (2003). Investigation of the projectile ion velocity inside the interaction media by the X-ray spectromicroscopy method. *Rev. Scien. Instr.* **74**, 5039–5045.

Rosmej, O.N., Blazevic, A., Korostiy, S., Bock, R., Hoffmann, D.H.H., Pikuz jr., S.A., Efremov, V.P., Fortov, V.E., Fertman, A., Mutin, T., Pikuz, T.A. & Faenov, A.Ya. (2005*a*). Charge state and stopping dynamics of fast heavy ions in dense matter. *Phys. Rev. A* **72**, 052901.

Rosmej, O.N., Pikuz jr., S.A., Korostiy, S., Blazevic, A., Brambrink, E., Fertman, A., Mutin, T., Shevelko, V.P., Efremov, V.P., Pikuz, T.A., Faenov, A.Ya., Loboda, P., Golubev, A.A. & Hoffmann, D.H.H. (2005*b*). Radiation dynamics of fast heavy ions interacting with matter. *Laser Part. Beams* **23**, 1–7.

Rozet, J.P., Stephan, C. & Vernhet, D. (1996). ETACHA: A program for calculating charge states at GANIL energies. *Nucl. Instr. Meth. Phys. Res. B* **107**, 67–70.

Safronova, U.I. & Lisina, T.G. (1979). Atomic constants of autoionizations states of ions with Z = 6, 8, 10–42 in Be isoelectronic sequence. *Atom. Data Nucl. Data* **24**, 49–93.

Shevelko, V.P. (1980). On the relation between quantum-mechanical and impact parameter amplitudes in charge exchange. *J. Phys. B* **13**, L319–L322.

Shevelko, V.P. (2001). Charge exchange in collisions between heavy low-charged ions. *Tech. Phys.* **46**, 1225–1234.

Shevelko, V.P., Tolstikhina, I.Y. & Stöhlker, T. (2001). Stripping of fast heavy low-charged ions in gaseous target. *Nucl. Instr. Meth. Phys. Res. B* **184**, 295–308.

Shevelko, V.P., Rosmej, O.N., Tawara, H. & Toltikhina, I.Yu. (2004). Target-density effect in electron-capture processes. *J. Phys. B: At. Mol. Opt. Phys.* **37**, 201–213.

Shevelko, V.P., Tawara, H., Ivanov, O.V., Miyoshi, T., Noda, K., Sato, Y., Subbotin, A.V. & Tolstikhina, I.Yu. (2005). Target density effects in collisions of fast ions with solid targets. *J. Phys. B: At. Mol. Opt. Phys.* **38**, 2675–2690.

Shima, K., Ishihara, T. & Mikumo, T. (1982). Empirical formula for the average equilibrium charge-state of heavy ions behind various foils. *Nucl. Instr. Meth. Phys. Res.* **200**, 605–608.

Sobelman, I.I. & Vainshtein, L.A. (2006). *Excitation of Atomic Spectra.* London: Alpha Science International Ltd.